

FIELD MATCHING OF F-D-F, GAP SHAPING MAGNETS FOR A 2 GeV CW FFA*

Wei Fu[†], Tianjue Zhang, Chuan Wang, Tianjian Bian, Hongji Zhou, Xiaofeng Zhu, Suping Zhang
 China Institute of Atomic Energy, P.O. Box 275(3), Beijing, China

Abstract

Fixed Field Alternating Gradient Accelerators have been developed for decades. A continuous wave (CW) 2 GeV FFA which aims at high-power proton beam applications is under developing in China Institute of Atomic Energy (CIAE). To avoid dangerous resonance lines and manipulate the tune diagram flexibly, 3rd order magnetic field is applied along the radius and 10-fold symmetrical F-D-F scheme has been proved to be feasible. In this paper, Integral Equation Method (IEM) is introduced and shown more efficient than adjusting the variable gap manually, saving time for magnet design. First of all, the radial mean field is set as a main design goal and the ΔH at different radii is solved by linear equations based on IEM. The isochronism is done when the mean field is well matched with the design value, whereas some precise corrections are needed for the oscillating frequency ν_r and ν_z , such as fringe field effects and multipole components near the end of pole face. The tune shift caused by fringe field is also included in this paper. Fringe field is more crucial for HTS magnets especially, since the leaked field of superconducting coil is ~ 1 kGs. Considering that, we apply an angular matching method to compensate the tune shift by fringe field.

INTRODUCTION

Continuous wave (CW) FFA which combines the characteristics of both cyclotrons and synchrotrons is a potential solution to provide MW proton beams for many important applications, such as accelerator driven subcritical system (ADS), neutron sources and neutrino factory [1]. CIAE launched the researches on CW FFAs in 2013 and proposed an energy efficient FFA design in 2019 [2]. High temperature superconducting (HTS) magnets and high-Q value RF cavities are adopted in the overall design of 2 GeV CW FFA, for a higher energy efficiency and less operating cost. Different types of magnets are presented for both scaling and non-scaling FFA, such as room temperature magnets [3], superferric magnets [4] (superconducting coils with warm iron) and iron-free superconducting magnets [5]. Gap shaping iron with HTS coils is applied in consideration of engineering convenience and operating cost. The 10-fold symmetrical F-D-F lattice design for the main machine is completed, which leads to next stage of magnet design. HTS magnets for FFA application are researched for several years and some experimental coils are wound to support engineering feasibility [6]. In practice, field matching is not crucial issue in FFA design. But for our non-

scaling 2 GeV FFA, which introduces third order field in wide range along radius, it is important to match the second and third order field to ensure isochronism and tune.

Moreover, fringing fields of entrance and exit side can affect the working diagram and result in tune shift, which requires prudent evaluation and compensation [3, 7], even if we match the mean field almost perfectly. This problem is more prominent in superconducting magnets and need to be well considered. Above all, the basic design of F-D-F lattice is introduced. The F-D-F lattice and static equilibrium orbits are shown in Fig. 1, in which red blocks represent focusing magnets and yellow block for defocusing magnet.

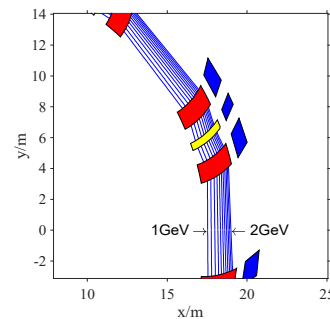


Figure 1: Layout of F-D-F magnets and static equilibrium orbits (1 GeV to 2 GeV).

Basic parameters of focusing and defocusing magnets are listed in Table 1.

Table 1: Parameters of Focusing and Defocusing Magnet

Item	Focusing magnet	Defocusing magnet
Pole length / m	2.1	2.1
Field range / T	1.57~2.66	-2.31~-1.15
Angular width / deg	4	1.6
Spiral angle / deg	0~36	0~36

ANALYTICAL MODEL

Approximation of Saturated Iron Blocks

In scaling FFAs, the magnetic field distribution is clear and defined using the Eq. (1) below:

$$B(r) = B_0 \left(\frac{r}{r_0} \right)^k. \quad (1)$$

Therefore, the gap shape is expressed by:

$$g(r) = g_0 \left(\frac{r}{r_0} \right)^k, \quad (2)$$

* Work supported by the National Natural Science Foundation of China under Grant 12135020 and the basic research fund from the Ministry of Finance of China under Grant BRF201901.

[†] fuwei@ciae.ac.cn.

simply. For CIAE 2 GeV FFA machine, though the peak field is described by 3rd order polynomial, the gap shape could be obtained in a similar way. However, magnetic field distribution of gap size which is attained Eq. (2) is far from accurate gap size due to complicated magnetization. Analogous to the shimming process of traditional cyclotrons, magnetic field of iron blocks which are located in different radius can be calculated using finite element method (FEM). In superferric magnets, due to the utilization of superconducting coils with higher current for excitation, some simplifications could be reasonable in calculating the field. In detail, the field in iron poles are close to saturation, which could be verified by FEM later. The state of iron magnetization can be regarded as saturated and the numerical calculation of small iron blocks with a cutting height of ΔH can be performed using the IEM. The field of saturated iron blocks is obtained by Eq. (3):

$$\mathbf{H}_m = \frac{1}{4\pi} \oint (\mathbf{M}_s \cdot \mathbf{n}) \frac{(\mathbf{r} - \mathbf{r}_i')}{|\mathbf{r} - \mathbf{r}_i'|^3} ds, \quad (3)$$

where \mathbf{M}_s is the magnetization and \mathbf{n} is the normal vector. The integration is implemented in both upper and lower surfaces of iron block as illustrated in Fig. 2.

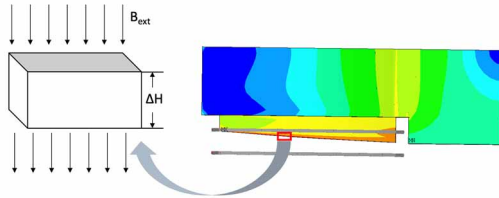


Figure 2: Schematic diagram of saturated iron blocks.

In view of this, IEM is more efficient than FEM to obtain the field caused by iron blocks. For simplicity, we assume that the magnetic field contribution from iron at different radius can be combined and the amplitude of field bump is linear to the height of iron block. The difference between the magnetic field required by the theoretical design and the magnetic field calculated by FEM can be expressed as ΔB in Eq. (4).

$$\Delta B(r) = \sum_{i=0}^n \alpha_i \Delta B_i(r) \quad (4)$$

To verify this approximation of saturation, two cases for uniform gap 0.1 m and 0.05 m are calculated. Comparisons between IEM and FEM calculated fields at different location of spiral magnet are shown in Fig. 3(a) and 3(b), while ΔH of each case is 10 mm. The amplitude of IEM result is different from FEM, which indicates that the saturated field is mutative with gap size. Adjustment coefficients of a series of gap sizes could be useful for more accurate calculation.

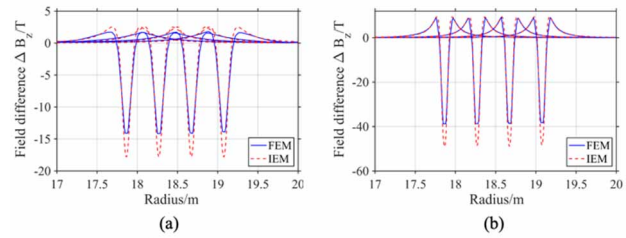


Figure 3: Comparison between IEM and FEM, two cases (a) gap = 0.1 m, (b) gap = 0.05 m.

Construction of Linear Equations System

The linear assumption mentioned above is only valid within a certain range of adjustment. If the range of the adjustment needs to be limited, linear programming (LP) method could be used to solve this problem. In other words, Eq. (4) could be transformed into following minimum optimization problem, shown in Eq. (5):

$$\begin{aligned} & \min \lambda \\ & \begin{cases} M \cdot \alpha - \lambda \leq 0 \\ -(M \cdot \alpha + \lambda) \leq 0, \\ \alpha_l \leq \alpha_i \leq \alpha_u \end{cases} \end{aligned} \quad (5)$$

where M is the coefficient matrix quantifies magnetic field caused by unit iron block, α_l and α_u are the upper and lower limits of the adjustment coefficient. The optimized goal λ stands for the maximum of field deviation. When the solution of this LP problem is found, optimal gap shape is obtained at the same time.

Fringe Field of Spiral Edges

Many analytical models have been proposed for fringe field of magnets. For convenience and conciseness, theoretical fields of F-D-F magnets adopts Enge function to model the fringe field. However, opposite field occurs near the edge of HTS magnet which makes it inaccurate using Enge function. Researchers have found that the variable gap is conflict with tuning of fringe field in scaling FFAs [3]. In our CW machine, mean field is set as matching goal to construct isochronous field primarily. For fringe field correction, the difference of flutter plays an important role in tune shift and high order contribution to vertical oscillation frequency is eliminated. Since the mean field has been well-matched with theoretical field distribution, only the $\langle B^2 \rangle$ items should be considered, which can be separated in Eq. (6) below.

$$\langle B^2 \rangle = \langle (B_f + B_d)^2 \rangle \approx \langle B_f^2 \rangle + \langle B_d^2 \rangle, \quad (6)$$

where B_f is the field of two focusing magnet, B_d is the field of one defocusing magnet. Consistent with the traditional effective length adjustment method, one can obtain an adjustment amount for the pole face length based on the flutter matching. The quantity of adjustment can be expressed as Eq. (7):

$$\Delta l = l' - l = l_d \frac{\int f_1^2(s) ds}{\int g^2(s) ds} - l, \quad (7)$$

where f and g are the normalized distribution function of focusing and defocusing magnet. Since function of distribution would change with pole length, correction process is carried out iteratively.

FIELD MATCHING RESULTS

Mean Field Matching in Radial direction

According to this IEM-based method, magnetic field differences between the FEM model and theoretical calculation are shown in Fig. 4, which illustrates that the relative error of the mean field can be minimized to 2%.

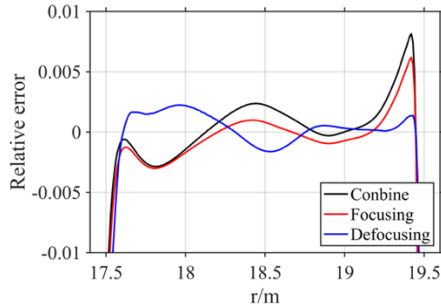


Figure 4: Radial mean magnetic field relative error.

Isochronism

Static beam dynamic of single particle is carried out to verify the FEM model. Differential and integral phase slip with FEM field is shown in Fig. 5 below, which indicates that average fields of FEM calculated field and theoretical design is matched well.

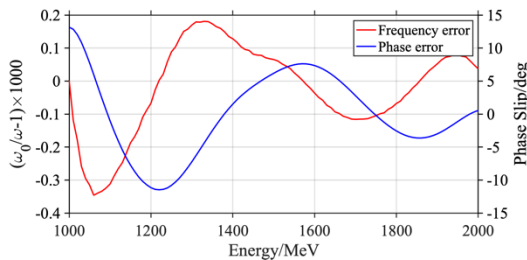


Figure 5: Differential and integral phase slip with FEM field.

Tune Diagram and Stable Regions

The tune diagram calculated by different FEM models is shown in the Fig. 6 below. The axial oscillation frequency is much higher than the design without any correction and the reason is the fringe field of the opposite direction. If we adopt the effective length correction mentioned in analytical equation, the working path is closer to the design result. Furthermore, the gap between design and FEM results can be narrowed with fringe field correction using Eq. (7). By adjusting the angular width, the change of flutter with the radius can be corrected, so that the axial working point calculated by finite element can be adjusted to the vicinity of the theoretically designed axial working point, which proves that the method is feasible.

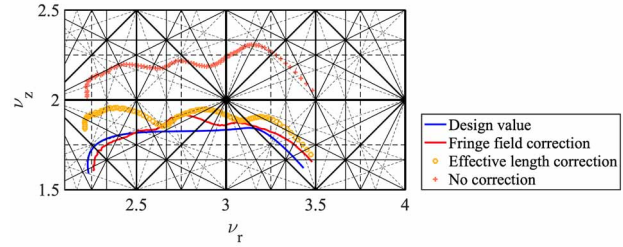


Figure 6: Tune diagram correction process.

Stable region for particle motion is also calculated based on FEM field. It can be seen from Fig. 7, that the dynamic aperture obtained by FEM calculation is not much different from the theoretical magnetic field for the resonance line of $3\nu_r = 10$; but for the high-order resonance $4\nu_r = 10$, the aperture obtained by finite element calculation is much smaller than theoretical value. The numerical error in the modelling and calculation process of the FEM magnetic field is the main reason, which leads to the local drastic change of the high-order driving term.

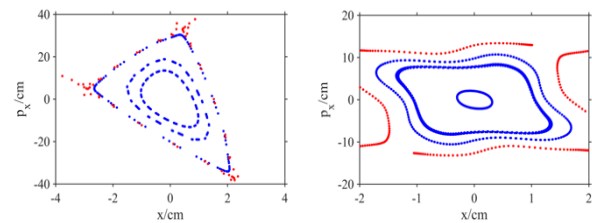


Figure 7: Stable phase region calculated with FEM field, $3\nu_r = 10$ (left), $4\nu_r = 10$ (right).

CONCLUSION

In this paper, a method for matching field distribution between FEM model and theoretical design is introduced. There are some problems coming with high field and compact scheme of magnet, such as fringe field and high order components. Two main problems have been solved, which are high order field matching and tune shift correction caused by fringe field. Particularly, the field matching result demonstrates relative error between design and FEM model is 2%, which guarantees the isochronism of whole machine. Based on this method, the gap between magnetic engineering and physical design is narrowed.

REFERENCES

- [1] C. Johnstone *et al.*, "Advances in nonlinear non-scaling FFAGs," *Int. J. Modern Phys. A*, vol. 26, no. 10-11, pp. 1690-1712, Apr. 2011. doi:10.1142/S0217751X11053110
- [2] T. J. Zhang *et al.*, "A New Solution for Cost Effective, High Average Power (2 GeV, 6 MW) Proton Accelerator and its R&D Activities", in *Proc. Cyclotrons'19*, Cape Town, South Africa, Sep. 2019, pp. 334-339. doi:10.18429/JACoW-CYCLOTRONS2019-FRA01

Content from this work may be used under the terms of the CC-BY-4.0 licence (© 2022). Any distribution of this work must maintain attribution to the author(s), title of the work, publisher, and DOI

- [3] T. Planche *et al.*, “Design of a prototype gap shaping spiral dipole for a variable energy proton therapy FFAG,” *Nucl. Instrum. Methods Phys. Res. Sect. A*, vol. 604, no. 3, pp. 435-442, 2009. doi:10.1016/j.nima.2009.02.026
- [4] B. Qin *et al.*, “Compact superferric FFAG accelerators for medium energy hadron applications,” *Nucl. Instrum. Methods Phys. Res. Sect. A*, vol. 648, no. 1, pp. 28-34, Aug. 2011. doi: 10.1016/j.nima.2011.05.035
- [5] T. Obana *et al.*, “Magnetic field design of a superconducting magnet for a FFAG accelerator,” *IEEE Trans. Appl. Supercond.*, vol. 15, no. 2, pp. 1185-1188, Jun. 2005. doi:10.1109/TASC.2005.849528
- [6] N. Amemiya *et al.*, “Research and development of fundamental technologies for accelerator magnets using high Tc superconductors,” *Physica C Supercond. Appl.*, vol. 482, no. 1, pp. 74-79, Nov. 2012. doi:10.1016/j.physc.2012.05.017
- [7] J. Fourrier *et al.*, “Spiral FFAG lattice design tools. Application to 6-D tracking in a proton-therapy class lattice,” *Nucl. Instrum. Methods Phys. Res. Sect. A*, vol. 589, no. 2, pp. 133-142, May 2008. doi:10.1016/j.nima.2008.01.082